Journal of Statistical Software

October 2011, Volume 44, Issue 12. *http://www.jstatsoft.org/*

Beyond the Gaussian Model in Diffusion-Weighted Imaging: The Package dti

Jörg Polzehl
WIAS Berlin

Karsten Tabelow
WIAS Berlin, MATHEON

Abstract

Diffusion weighted imaging (DWI) is a magnetic resonance (MR) based method to investigate water diffusion in tissue like the human brain. Inference focuses on integral properties of the tissue microstructure. The acquired data are usually modeled using the diffusion tensor model, a three-dimensional Gaussian model for the diffusion process. Since the homogeneity assumption behind this model is not valid in large portion of the brain voxel more sophisticated approaches have been developed.

This paper describes the R package **dti**. The package offers capabilities for the analysis of diffusion weighted MR experiments. Here, we focus on recent extensions of the package, for example models for high angular resolution diffusion weighted imaging (HARDI) data, including Q-ball imaging and tensor mixture models, and fiber tracking. We provide a detailed description of the package structure and functionality. Examples are used to guide the reader through a typical analysis using the package. Data sets and R scripts used are available as electronic supplements.

Keywords: diffusion weighted imaging, high angular resolution, orientation distribution function, Q-ball imaging, angular central Gaussian distribution, tensor mixture model, order selection.

1. Introduction

The basic principles of diffusion weighted imaging (DWI) have been introduced in the 1980's (Le Bihan and Breton 1985; Merboldt *et al.* 1985; Taylor and Bushell 1985). Since then it has evolved into a beneficial technique for in-vivo investigation of tissue micro-structure in the human brain (Le Bihan *et al.* 2001), spinal cord (Clark *et al.* 1999) and muscle tissue (Sinha *et al.* 2006) as it probes microscopic structures well beyond typical image resolutions through water molecule displacement. Diffusion weighted data is usually measured using the pulsed gradient spin echo sequence (PGSE, Stejskal and Tanner 1965) with a number of specified

magnetic field gradients in different directions $\vec{q}$. Due to diffusion in tissue this signal $S(\vec{q})$ is attenuated compared to the signal S_0 acquired without diffusion gradient application. For a recent discussion of the physics of image acquisition, relations to white matter anatomy, clinical use and problems in neuroscience that can be addressed by DWI we refer to Johansen-Berg and Behrens (2009). A good introduction into the basic principles of magnetic resonance imaging is given in Callaghan (1991). Requirements on DTI acquisition schemes are discussed e.g., in Smith *et al.* (2007).

In this paper we discuss the modeling and analysis of single subject DWI data after image reconstruction using the package **dti** (Tabelow and Polzehl 2011) for the R environment for statistical computing (R Development Core Team 2011). An earlier version (0.6-0) of the package that was restricted to diffusion tensor imaging (DTI) and adaptive smoothing for DTI (Tabelow *et al.* 2008) has been described in Polzehl and Tabelow (2009).

The focus of this paper is on models for estimating the orientation distribution function (ODF), see Tuch *et al.* (2002); Wedeen *et al.* (2005); Aganj *et al.* (2010) and Barnett (2009), that overcome the limitations of the tensor model. Such models are of special interest for high angular resolution diffusion weighted imaging (HARDI) data. Section 2.2 briefly reviews the diffusion tensor model and discusses its limitations. We then introduce both Q-ball imaging (Tuch 2004; Anderson 2005; Hess *et al.* 2006; Descoteaux *et al.* 2007) and tensor mixture models (Tuch 2002; Tournier *et al.* 2004; Alexander 2005; Özarslan *et al.* 2006; Alexander 2006; Behrens *et al.* 2007; Leow *et al.* 2009; Tabelow *et al.* 2011b). Section 4 introduces the design of the package and uses several examples to illustrate a typical data analysis. Data sets and R scripts are provided in electronic form.

2. Modeling diffusion weighted data

2.1. The diffusion weighted signal

DWI effectively measures the diffusion of water molecules in a direction determined by external magnetic field gradients. Let $P(\vec{r}, \vec{r}', \tau)$ denote the probability density for a particle (spin) to diffuse from position $\vec{r}'$ to $\vec{r}$ in time τ. With DWI an aggregate value of P over a volume (voxel) V can be determined,

$$P(\vec{R}, \tau) = \int_{\vec{r}' \in V,\ \vec{R}=\vec{r}-\vec{r}'} P(\vec{r}, \vec{r}', \tau) p(\vec{r}') d\vec{r}', \tag{1}$$

where $p(\vec{r}')$ is the initial probability density of the location of the particles. A voxel is typically of a size of about $1 - 8$ mm^3. The relation to the normalized diffusion weighted signal $E(\vec{q}, \tau) = S(\vec{q}, \tau)/S_0$, is given by the three-dimensional Fourier transform $\mathcal{F}$ and its inverse:

$$\begin{aligned} P(\vec{R}, \tau) &= \int_{\mathbb{R}^3} E(\vec{q}, \tau)\ e^{-2\pi i \vec{q}\vec{R}} d\vec{q} = \mathcal{F}(E(\vec{q}, \tau)), \\ E(\vec{q}, \tau) &= \int_{\mathbb{R}^3} P(\vec{R}, \tau)\ e^{2\pi i \vec{q}\vec{R}} d\vec{R} = \mathcal{F}^{-1}(P(\vec{q}, \tau)). \end{aligned} \tag{2}$$

Figure 1 provides a snapshot of a three dimensional data visualization generated by

Figure 1: 3D Data visualization for a row of four voxel in the artificial tensor data using the package **rgl** (Adler and Murdoch 2010). For each voxel the values $E(\vec{q}, \tau)$ are coded as distances to voxel centers. Diffusion gradients are characterized by their spherical coordinate directions and additional color coding using red for left-right, green for anterior-posterior and blue for inferior-superior directions.

```
R> library("dti")
R> data("optgradients")
R> gradients <- cbind(matrix(0, 3, 1), optgrad[[16]])
R> dwiobj <- readDWIdata(gradients, "data3", "NIFTI")
R> show3d(dwiobj[26:30, 26, 15], bg = "white", what = "data")
R> rgl.snapshot("dwidata.png")
```

Within a DWI experiment n_{grad} diffusion weighted images $S(\vec{q}_i, \tau)$ and at least one image S_0 without application of a diffusion gradient are acquired (Smith *et al.* 2007).

2.2. The diffusion tensor model

Assuming homogeneity of tissue within a voxel the diffusion tensor model is derived for the special case of Gaussian diffusion[1], that is fully characterized by a three dimensional tensor $\mathcal{D}$,

$$P(\vec{R}, \tau) = P(r\vec{u}, \tau) = \frac{1}{\sqrt{\det \mathcal{D}(4\pi\tau)^3}} \exp\left(-r^2 \frac{\vec{u}^\top \mathcal{D}^{-1} \vec{u}}{4\tau}\right).$$

Equation 2 can then be expressed as

$$E(\vec{q}, \tau) = E(q\vec{u}, \tau) = e^{-b\vec{u}^\top \mathcal{D}\vec{u}},$$

with the b value depending on q and the effective diffusion time τ (Basser *et al.* 1994a). Within this model diffusion is completely characterized by the positive definite symmetric 3×3 matrix $\mathcal{D}$, the diffusion tensor. For simplicity of notation we henceforth omit the diffusion time τ.

The components of the diffusion tensor clearly depend on the orientation of the object in the scanner frame. Rotationally invariant quantities derived from the diffusion tensor circumvent

[1]Free diffusion is usually isotropic except in some liquid crystals. However, the Gaussian model of anisotropic diffusion can be considered as the low spatial frequency approximation to the diffusion propagator in case of restricted diffusion (Tuch *et al.* 2002).

this dependence and are usually used for further analysis, mainly based on the eigenvalues λ_i ($i = 1, 2, 3$) of $\mathcal{D}$ with $\lambda_i > 0$ for positive definite tensors (Basser and Jones 2002). The eigenvector $\vec{e}_1$ corresponding to the principal eigenvalue λ_1 determines the main diffusion direction used for fiber tracking.

The simplest quantity based on the eigenvalues is the trace of the diffusion tensor $\mathrm{Tr}(\mathcal{D}) = \sum_{i=1}^{3} \lambda_i$ which is related to the mean diffusivity $\langle\lambda\rangle = \mathrm{Tr}(D)/3$. The anisotropy of the diffusion can be described using higher moments of the eigenvalues λ_i. The widely used fractional anisotropy (FA) is defined as

$$\mathrm{FA} = \sqrt{\frac{3}{2}} \sqrt{\sum_{i=1}^{3} (\lambda_i - \langle\lambda\rangle)^2 \;/\; \sum_{i=1}^{3} \lambda_i^2},$$

with $0 \leq \mathrm{FA} \leq 1$, where $\mathrm{FA} = 0$ indicates equal eigenvalues and hence isotropic diffusion.

The resulting FA-maps together with a color-coding scheme are used for visualization and interpretation. Clinical use focuses on diagnostics of neuronal disease, see e.g., Kellinghaus *et al.* (2006); Kleffner *et al.* (2008); Deppe *et al.* (2008); Duning *et al.* (2010). The principal eigenvector $\vec{e}_1 = (e_{1x}, e_{1y}, e_{1z})$ is used for assigning each voxel a specific color, interpreting e_{1x}, e_{1y}, and e_{1z} weighted with the value FA as red (left-right), green (anterior-posterior), and blue (inferior-superior) contribution

$$(R, G, B) = (|e_{1x}|, |e_{1y}|, |e_{1z}|) \cdot \mathrm{FA}\,. \tag{3}$$

Note, that in contrast to the eigenvalues and the FA the principal eigenvector, and hence the color coding, depends on the orientation of the object in the scanner frame.

The main problem of the diffusion tensor model arises from the assumption of tissue homogeneity within a voxel. DWI aims to detect structures with an extension of up to 15 cm and a diameter of about 30 μm. A high percentage of voxels contain structures with different orientations. In such a situation partial volume effects may lead to invalid or non-informative tensor estimates.

2.3. The orientation distribution function

The drawbacks of the diffusion tensor model may be avoided by a more detailed analysis of Equation 1. The main concern in DWI is to access properties of the tissue like neuronal fiber bundles. A special interest is in the orientation properties of the probability distribution P (its projection onto the unit sphere $\mathbb{S}^2$)

$$\mathrm{ODF}(\vec{u}) = \int_0^\infty r^2 P(r\vec{u}) dr, \tag{4}$$

with $\vec{R} = r\vec{u}$ and $\vec{u} \in \mathbb{S}^2$ and neglecting the dependence on τ. Equation 4 is the orientation distribution function (ODF) as proposed in Wedeen *et al.* (2005) and used in Aganj *et al.* (2010). For a detailed discussion on how this differs from the original definition of Tuch *et al.* (2002) see Barnett (2009). This definition is intrinsically normalized

$$\int_{\mathbb{S}^2} \mathrm{ODF}(\vec{u}) d\vec{u} = 1,$$

and defines a probability distribution on the sphere $\mathbb{S}^2$.

In case of elliptically symmetric distributions $P(\vec{R}, \tau) = C_\tau (\det \mathcal{D})^{-1/2} h_\tau(\vec{R}^\top \mathcal{D}^{-1} \vec{R})$ with zero mean, a three dimensional tensor $\mathcal{D}$ as shape parameter, some function h_τ and a normalization constant C_τ the ODF is given by

$$\mathrm{ODF}(\vec{u}) = \frac{1}{4\pi\sqrt{\det \mathcal{D}}} \left(\vec{u}^\top \mathcal{D}^{-1} \vec{u}\right)^{-3/2},$$

(see Tabelow *et al.* 2011b). This is known as the *angular central Gaussian distribution* on the sphere (Mardia and Jupp 2000). One example for an elliptically symmetric distribution P is the anisotropic Gaussian diffusion assumed for the tensor model.

Using spherical coordinates $\vec{q} = q\vec{u} = (q, \theta, \phi)$ and inserting (2) into (4) the orientation distribution function may be expressed as a function of the signal $E(\vec{q})$:

$$\mathrm{ODF}(\vec{u}) = \frac{1}{4\pi} - \frac{1}{8\pi^2} \int_0^{2\pi} \int_0^{\infty} \frac{1}{q} \nabla_b^2 E(\vec{q}) dq d\phi$$
$$\nabla_b^2 E = \frac{1}{\sin\theta} \frac{\delta}{\delta\theta} \left(\sin\theta \frac{\delta E}{\delta\theta}\right) + \frac{1}{\sin^2\theta} \frac{\delta E}{\delta\phi^2}$$

where ∇_b^2 is the Laplace-Beltrami operator (Aganj *et al.* 2010).

2.4. Q-ball imaging

Q-ball imaging (QBI, Tuch 2004) aims at the reconstruction of the ODF from signals $E(\vec{q}_0)$ measured on one q-shell, i.e., for one fixed b value corresponding to the value q_0. This is in contrast to alternative methods like diffusion spectrum imaging (DSI, Wedeen *et al.* 2005) or hybrid diffusion imaging (HYDI, Wu and Alexander 2007) which measure diffusion weighted images on a Cartesian grid of diffusion gradients or sample gradients from spheres with different b values, respectively. Both methods effectively require significantly more diffusion weighted images.

QBI requires an extrapolation of the signal $E(\vec{q})$ to other locations in q-space in order to evaluate the integral over q. Here, we use the formulation of QBI as in Aganj *et al.* (2010) which differs from the original proposal by Tuch (2004) by the r^2 weighting factor in the definition of the ODF. The extrapolation of $E(\vec{q}_0)$ is performed by assuming a mono-exponential decay of the signal in q

$$E(q\vec{u}) = E(q_0\vec{u})^{(q/q_0)^2}.$$

Under this assumption the ODF may be expressed as

$$\mathrm{ODF}(\vec{u}) = \frac{1}{4\pi} + \frac{1}{16\pi^2} \mathrm{FRT}\{\nabla_b^2 \ln(-\ln E(\vec{u}))\},$$

where

$$\mathrm{FRT}(f(\vec{u})) = \iint_{\vec{u}^\perp} f(\vec{w}) \delta(|\vec{w}| - 1) d\vec{w}$$

denotes the Funk-Radon transformation (Aganj *et al.* 2010).

Efficient implementations of QBI make use of the spherical harmonic basis functions $Y_k^m(\vec{u})$, particularly in the form of the a symmetric modified basis. For selected maximum order l,

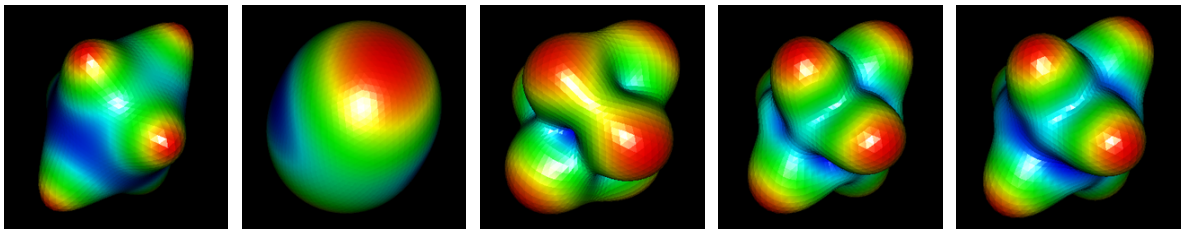

Figure 2: True ODF and expected reconstruction by spherical harmonics expansion of order 2, 4, 6 and 8 (from left to right) for a voxel with tree mixture components.

even order $k \leq l$, and $-k \leq m \leq k$ we define an index $j = k(k+1)/2 + m + 1$ and a real function

$$Y_j(\vec{u}) = \begin{cases} \sqrt{2}\Re(Y_k^m(\vec{u})) & -k \leq m < 0; \\ Y_k^0(\vec{u}) & m = 0; \\ \sqrt{2}\Im(Y_k^m(\vec{u})) & 0 < m \leq k; \end{cases}$$

using the real part $\Re(Y_k^m(\vec{u}))$ and the imaginary part $\Im(Y_k^m(\vec{u}))$ of $Y_k^m(\vec{u})$ (Descoteaux *et al.* 2007). The spherical harmonics Y_j are eigenfunctions of the Laplace-Beltrami operator, i.e., $\nabla_b^2 Y_j(\vec{u}) = -k_j(k_j+1)Y_j(\vec{u})$, where k_j is the order associated with j. The use of the expansion

$$\ln(-\ln(E(\vec{u}))) \approx \sum_{j=1}^{N} c_j Y_j(\vec{u}), \qquad N = (l+1)(l+2)/2, \tag{5}$$

leads to an approximation of the ODF by

$$\mathrm{ODF}(\vec{u}) \approx \frac{1}{4\pi} - \frac{1}{8\pi} \sum_{j=1}^{N} c_j k_j (k_j+1) P_{k_j}(0) Y_j(\vec{u}) \tag{6}$$

where P_{k_j} are the Legendre polynomials of order k_j (Aganj *et al.* 2010). Estimation of the ODF is now a linear problem where estimates of the parameters $c_j,\ j = 1, \ldots, N$ are obtained from the observed noisy signals $E(\vec{u}_i) = S(\vec{q}_i)/S_0,\ i = 1, \ldots, n_{grad}$ by solving the regularized least squares problem (Descoteaux *et al.* 2007; Aganj *et al.* 2010)

$$\min_{(c_1,\ldots,c_N)} \sum_{i=1}^{n_{grad}} \left(\ln(-\ln(E(\vec{u}_i))) - \sum_{j=1}^{N} c_j Y_j(\vec{u}) \right)^2 + \lambda_{reg} \sum_{j=1}^{N} c_j^2 k_j^2 (k_j^2+1).$$

Regularization is used to reduce the variability of the estimated ODF, with the parameter λ_{reg} effectively determining a balance between variance and bias of the estimated ODF. Figure 2 illustrates effects of ODF reconstruction by spherical harmonic expansions for a voxel where the true ODF is a mixture of three angular central Gaussian distributions. Reconstruction was based on 136 gradient directions in a noise-free situation. Figure 2 is generated using the following script.

```
R> data("optgradients")
R> gradients <- cbind(matrix(0, 3, 7), optgrad[[131]])
R> dwiobj <- readDWIdata(gradients, "data4a", "NIFTI")
```

```
R> mixtens3 <- dwiMixtensor(dwiobj[5, 5, 5], maxcomp = 5, pen = 1)
R> qballobj2 <- dwiQball(dwiobj[5, 5, 5], order = 2, lambda = 0)
R> qballobj4 <- dwiQball(dwiobj[5, 5, 5], order = 4, lambda = 0)
R> qballobj6 <- dwiQball(dwiobj[5, 5, 5], order = 6, lambda = 0)
R> qballobj8 <- dwiQball(dwiobj[5, 5, 5], order = 8, lambda = 0)
R> source(system.file("rcode/mousecallbacks.r", package = "dti"))
R> sx <- 320
R> sy <- 320
R> w1 <- show3d(mixtens3, subdivide = 4, FOV = 1,
+    windowRect = c(1, 1, sx, sy))
R> w2 <- show3d(qballobj2, subdivide = 4, FOV = 1,
+    windowRect = c(sx + 11, 1, 2 * sx + 10, sy))
R> w3 <- show3d(qballobj4, subdivide = 4, FOV = 1,
+    windowRect = c(2 * sx + 21, 1, 3 * sx + 20, sy))
R> w4 <- show3d(qballobj6, subdivide = 4, FOV = 1,
+    windowRect = c(3 * sx + 31, 1, 4 * sx + 30, sy))
R> w5 <- show3d(qballobj8, subdivide = 4, FOV = 1,
+    windowRect = c(4 * sx + 41, 1, 5 * sx + 40, sy))
R> mouseTrackball(dev = c(w1, w2, w3, w4, w5))
R> mouseZoom(2, dev = c(w1, w2, w3, w4, w5))
R> mouseFOV(3, dev = c(w1, w2, w3, w4, w5))
R> cat("w1 - true ODF \n
+  w2 - Expected ODF estimate by SH approximation order 2, no regularization\n
+  w3 - Expected ODF estimate by SH approximation order 4, no regularization\n
+  w4 - Expected ODF estimate by SH approximation order 6, no regularization\n
+  w5 - Expected ODF estimate by SH approximation order 8, no regularization\n
+  You may now rotate the data using your mouse")
R> rgl.set(w1)
R> rgl.snapshot("truemix3.png")
R> rgl.set(w2)
R> rgl.snapshot("ExpectedODF2.png")
R> rgl.set(w3)
R> rgl.snapshot("ExpectedODF4.png")
R> rgl.set(w4)
R> rgl.snapshot("ExpectedODF6.png")
R> rgl.set(w5)
R> rgl.snapshot("ExpectedODF8.png")
```

Note, that ODF reconstruction by function `dwiQball` requires the package **gsl** (Hankin 2006).

2.5. Tensor mixture models

Although the estimation of the ODF by spherical harmonics expansion of the observed signal is computationally appealing it also has several drawbacks. The form of the ODF reconstruction depends on the order l of the approximation and the regularization parameter λ_{reg}. The approximation by orthogonal basis functions aims for a minimal mean squared error of the density estimates and may lead to a bias in the location of the maxima of the estimated ODF.

Finally, in the case of QBI, the result depends on the assumption of a mono-exponential decay of the signal E with q. One may therefore consider alternative models for DWI.

Let us assume a voxel to contain M compartments covering a fraction w_m of the voxel such that $\sum_{m=1}^{M} w_m = 1$ and anisotropic Gaussian diffusion characterized by the tensor $\mathcal{D}_m$ in compartment m, $m = 1, \ldots, M$. This leads to a signal that does not exhibit a mono-exponential decay but instead satisfies

$$E(\vec{q}) = \sum_{m=1}^{M} w_m \exp(-b\vec{u}^\top \mathcal{D}_m \vec{u}). \tag{7}$$

The corresponding ODF is a mixture of the ODF's for the compartments

$$\mathrm{ODF}(\vec{u}) = \sum_{m=1}^{M} w_m \frac{1}{4\pi\sqrt{\det \mathcal{D}_m}} \left(\vec{u}^\top \mathcal{D}_m^{-1} \vec{u}\right)^{-3/2}.$$

This additivity of the ODF is not preserved when using Equations 5 and 6 due to the non-linearity of the operators $\ln(-\ln(\cdot))$.

The mixture model of M diffusion tensors $\mathcal{D}_m$ in its general form (7) is too flexible, leading to severe identifiability and numerical problems (Tuch 2002; Johansen-Berg and Behrens 2009). Suggestions to resolve the problem include the restriction of the number of components to $M = 2$ (Alexander 2005, 2006; Özarslan *et al.* 2006), the approximation of the solution by estimating the ODF spherical harmonics expansion and subsequent deconvolution (Tournier *et al.* 2004) or the use of restrictions for the tensor eigenvalues (Leow *et al.* 2009).

In Tabelow *et al.* (2011b) we show that a reduction of the complexity of the model 7 accompanied by model selection using BIC (Schwarz 1978) is practical. We assume the diffusion tensors $\mathcal{D}_m$ to have a spectral decomposition $\mathcal{D}_m = \lambda_1 \vec{d}_m \vec{d}_m^\top + \lambda_2 (I_3 - \vec{d}_m \vec{d}_m^\top)$, i.e. to be prolate ($\lambda_1 > \lambda_2 = \lambda_3$, Basser *et al.* 1994b) and to differ only in their main direction $\vec{d}_m$. After re-parameterization the reduced model has the form

$$E(\vec{q}) = \sum_{m=1}^{M} \tilde{w}_m \exp(-b\vartheta(\vec{q}^\top \vec{d}_m)^2), \quad \tilde{w}_m \geq 0, \quad \sum_{m=1}^{M} \tilde{w}_m < 1, \quad \vartheta \geq 0, \tag{8}$$

with

$$\lambda_2 = -\frac{1}{b} \log \sum_{m=1}^{M} \tilde{w}_m, \quad \lambda_1 = \vartheta + \lambda_2 \quad \text{and} \quad w_m = \tilde{w}_m / \sum_{l=1}^{M} \tilde{w}_l.$$

With $\vec{d}_m = (\sin(\phi_m)\cos(\eta_m), \sin(\phi_m)\sin(\eta_m), \cos(\phi_m))^\top$ the model has $2M + 1$ nonlinear parameters and M linear parameters with constraints. Estimation in model 8 still requires to solve a non-convex optimization problem and the use of suitable initial estimates. For a detailed description of parameter estimation and a strategy to select the number of mixture components M we refer to Tabelow *et al.* (2011b). The tensor mixture model is characterized by the number of compartments M_{opt} estimated by BIC, the fractional anisotropy of a prolate tensor model

$$\mathrm{FA} = \frac{(\lambda_1 - \lambda_2)}{\sqrt{\lambda_1^2 + 2 \cdot \lambda_2^2}},$$

and, assuming $w_1 \geq \cdots \geq w_{M_{opt}}$, the effective order

$$\mathrm{EO} = \sum_{m=1}^{M_{opt}} (2m-1) w_m \; .$$

The definition of FA is a straightforward generalization from the DTI model. The value of EO ranges from 1 for $w_1 = 1$ to M_{opt} in case of equal mixture coefficients $w_m \equiv 1/M_{opt}$.

In general estimation in model 8 is computationally expensive and may require multiple starting points in optimization to provide suitable results.

2.6. Fiber tracking

The estimated diffusion tensors and ODF's may be used to infer the underlying neuronal fiber structure. This is performed using fiber tracking algorithms on vector fields or tensor orientation functions extracted from the estimated objects. There exists a large variety of fiber tracking algorithms that can be roughly classified into deterministic and probabilistic approaches and are based either on local or global criteria. For an overview of existing approaches, see e.g., Mori and van Zijl (2002); Behrens *et al.* (2007); Descoteaux *et al.* (2009); Reisert *et al.* (2011); Wu *et al.* (2009); Zhang *et al.* (2009); Aganj *et al.* (2011). For this paper we use the deterministic FACT algorithm proposed in Xue *et al.* (1999); Mori *et al.* (1999) and implemented in the **dti** package.

3. Data sets

With this document we provide four data sets that have been used within the text and may be used to explore the capabilities of the R package **dti**. The data are contained in the electronic appendix of this paper in form of directories containing NIfTI files. The data may be freely used under the terms of the GPL ≥ 2 license.

MRI images were obtained from a healthy male volunteer in the age group 40 - 45 within an Institutional Review Board approved research protocol at Weill Cornell Medical College. Images were acquired on a 3.0 Tesla General Electric Excite MRI scanner using an 8-channel receive-only head coil. First, a localizer scan was obtained to prescribe the position of the subsequent DWI scan. For the DWI scan, a single-shot spin-echo echo planar imaging (EPI) sequence with 10 images without diffusion weighting and 140 diffusion gradient directions, which were approximately isotropically distributed over the sphere, was used, with an echo and repetition time of TE = 73.2 ms and TR = 14000 ms, respectively. 66 axial slices were scanned with no gap and an acquisition matrix size of 128×128. Images were zero-filled to an image matrix size of 256×256, yielding an effective resolution of $0.898 \times 0.898 \times 1.800\,\mathrm{mm}^3$. The b value in the diffusion weighted images was 1000 s / mm^2, the parallel imaging acceleration factor was 2, and the total scan time for this scan was 36 min.

Experimental data 1: This data set contains a subset of the DWI data described above. The data covers parts of the genu of the corpus callosum (GCC), the anterior thalamic radiation (ATR) and the superior fronto-occipital-fasciculus (SFO).

Data directory:	`data1`
Dimension:	$40 \times 40 \times 5$

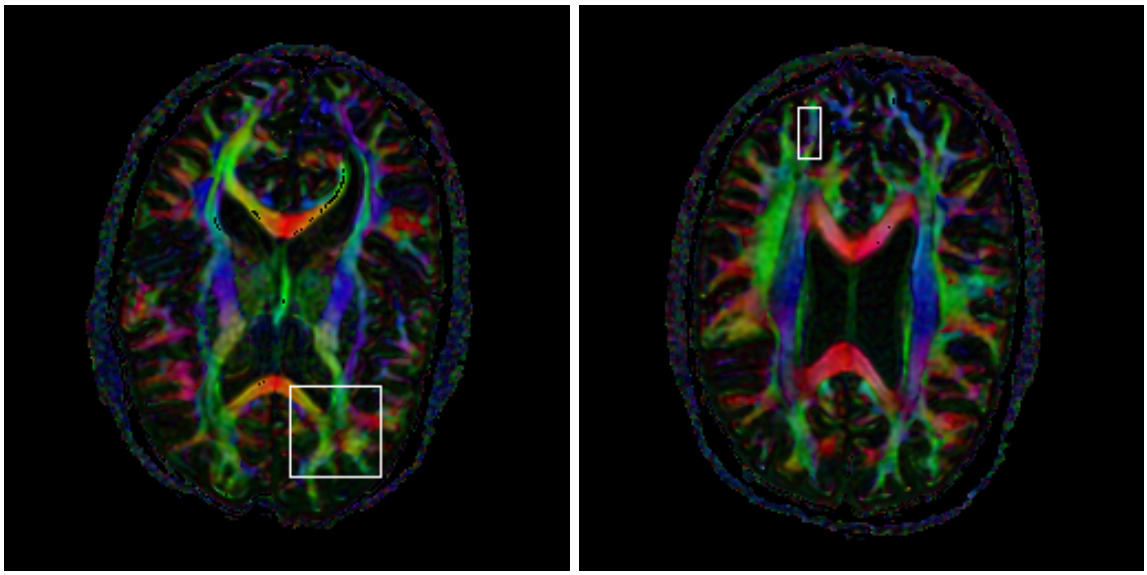

Figure 3: Color-coded FA with location for data cubes of the experimental data set 1 (left) and the experimental data set 2 (right). Information shown is within slice three of the respective subsets.

Gradient file:	`b-directions.txt`
Number of gradients n_{grad}:	140
S_0 images:	10

Experimental data 2: This data set contains a subset of the DWI data described above. The subset contains a contiguous region of tissue where three main directions of diffusion are found in the tensor mixture model.

Data directory:	`data2`
Dimension:	$9 \times 22 \times 5$
Gradient file:	`b-directions.txt`
Number of gradients n_{grad}:	140
S_0 images:	10

Figure 3 illustrates the position of the subsets in the experimental data set 1 (left) and the experimental data set 2 (right) using color coded FA maps for slices containing the central slice within the subsets, respectively.

Artificial tensor data: An artificial data set created by `demo("dti_art")` with default settings. For this data set the tensor model is adequate.

Data directory:	`data3`
Dimension:	$64 \times 64 \times 30$
Number of gradients n_{grad}:	21
S_0 images:	1
Gradient file:	access from package by

```
R> data("optgradients")
R> gradients <- cbind(matrix(0,3,1), optgrad[[16]])
```

Artificial tensor mixture data: An artificial data set created by `demo("mixtens_art")` with default settings (except $n = 7$).

Data directory:	`data4a` (without noise) and `data4b` (with $SNR = 50$)
Dimension:	$7 \times 7 \times 7$
Number of gradients n_{grad}:	136
S_0 images:	7
Gradient file:	access from package by

```
R> data("optgradients")
R> gradients <- cbind(matrix(0, 3, 7), optgrad[[131]])
```

Estimated fiber tracks: This data set contains fiber tracks identified from whole brain data recorded within an diffusion weighted experiment using a tensor mixture model of maximal order 3. (The experimental data sets 1 and 2 contain part of data from this experiment.) The data set contains fibers extending over at least 100 voxels. Access data using `load("tracks3_100.rsc")`.

4. Analyzing DWI data: The R package dti

The R package **dti** has been designed to perform an analysis of single subject diffusion weighted imaging data using S4 classes (Chambers 2008). The concept of S4 classes enables the use of principles from object oriented programming like inheritance, methods and polymorphism in R. Consistency of the work flow for analyzing DWI data (Figure 4) is guaranteed by well

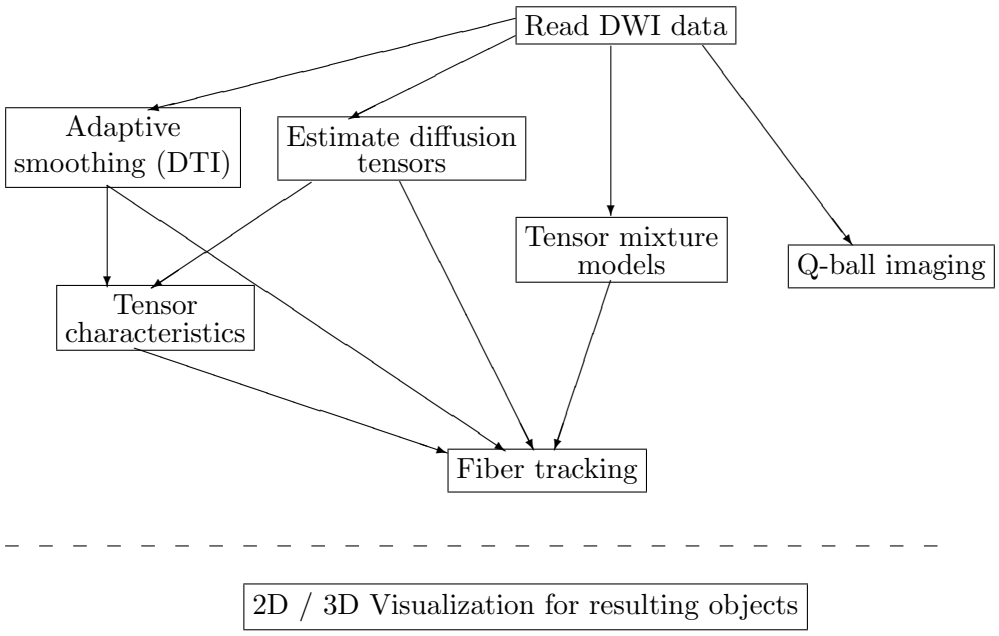

Figure 4: Work flow for analyzing DWI data with package **dti**.

Class	Content	ID
`dwi`	Basic class containing data description	(1)
`dtiData`	DWI data objects. Extends (1).	(2)
`dtiTensor`	Estimated diffusion tensor. Extends (1).	(3)
`dtiIndices`	Estimated diffusion tensor indices and orientations. Extends (1).	(4)
`dwiMixtensor`	Estimated tensor mixtures. Extends (1).	(5)
`dwiQball`	Estimated ODF using spherical harmonics. Extends (1).	(6)
`dwiFiber`	Fiber tracking results. Extends (1).	(7)

Table 1: Overview of package **dti**: Classes. A new class inherits the complete structure of the class that it extends.

Function	Purpose	Defined for	Creates
`dtiData`	Create DWI data from binary image file.		(2)
`readDWIdata`	Read DWI data using capabilities of **fmri**.		(2)
`sdpar`	Threshold selection and variance parameters.	(2)	(2)
`tensor2medinria`	Write tensor estimates as NIfTI.	(3)	
`medinria2tensor`	Read tensor estimates from NIfTI.		(3)

Table 2: Overview of package **dti**: Functions.

Method	Purpose	Defined for	Creates
`dtiTensor`	Compute diffusion tensor estimates.	(2)	(3)
`dti.smooth`	Adaptive smoothing for DTI.	(2)	(3)
`dtiIndices`	Compute diffusion tensor characteristics.	(3)	(4)
`dwiQball`	Q-ball imaging using spherical harmonics.	(2)	(6)
`dwiMixtensor`	Estimate tensor mixtures.	(2)	(5)
`dwiMtImprove`	Improve estimated tensor mixtures.	(5)(2)	(5)
`dwiMtCombine`	Combine estimated tensor mixtures.	(5)(5)	(5)
`tracking`	Streamline fiber tracking.	(3,4,5)	(7)
`selectFibers`	Select subset of fiber tracks.	(7)	(7)
`reduceFibers`	Remove redundant fiber tracks.	(7)	(7)
`extract`	Extract information or components.	(2,3,4,5,6)	
`[`	Index operations.	(2,3,4,5,6)	(2,3,4,5,6)
`summary`	Summarize information.	(2,3,4,5,6,7)	
`plot`	Plot method.	(2,3,4,5,7)	
`show`	Object descriptions.	(2,3,4,5,6,7)	
`print`	Object descriptions.	(2,3,4,5,6,7)	
`show3d`	3D visualization of objects.	(2,3,4,5,6,7)	

Table 3: Overview of package **dti**: Methods.

defined data structures and methods. Table 1 provides an overview of currently implemented classes. Table 2 lists the available functions and the classes of objects they generate. Table 3 gives a list of available methods and the respective classes of objects they act on and create. An extract method is provided to access specific information from the S4-objects, see Example 4.3. The information to extract is specified by an argument `what`. For detailed information we refer to the documentation of the package. The use of the package in DTI and our approach to

adaptive smoothing within this context is described in detail in Polzehl and Tabelow (2009); Tabelow *et al.* (2008).

Information on the package and its classes and methods is obtained within an R session by

```
R> help(dti)
R> class?class-name
R> methods?method-name
```

The package includes two data sets: `"polyeder"` contains a description of regular polyhedra that are refinements of the icosahedron and are used for visualization and `"optgradients"` contains sets of optimal gradient directions.

Currently there are two comprehensive demos, `demo("dti_art")` for modeling within the context of the diffusion tensor model and `demo("mixtens_art")` illustrating the work flow for analyzing HARDI data. In both demos a variety of configurations may be specified both concerning underlying true fiber structures as well as the number of gradients and signal-to-noise ratio (SNR).

4.1. Example: Tensor estimates

To illustrate the capabilities of the package in DTI in an adequate situation we use the artificial tensor data. The true structure has, in the anisotropic parts, main eigenvectors of the diffusion tensors along circular bands, and in the center, in vertical direction. Voxel-wise tensor estimates are obtained without and with structural adaptive smoothing (Tabelow *et al.* 2008; Polzehl and Tabelow 2009) using a maximal bandwidth of 4. Tensor characteristics are computed and fiber tracking is performed.

```
R> data("optgradients")
R> gradients <- cbind(matrix(0, 3, 1), optgrad[[16]])
R> dwiobj <- readDWIdata(gradients, "data3", "NIFTI")
R> dwiobj <- sdpar(dwiobj, 100)
R> dtiobj <- dtiTensor(dwiobj)
R> dtiind <- dtiIndices(dtiobj)
R> dtiobj.smooth <- dti.smooth(dwiobj, hmax = 4)
R> dtiind.smooth <- dtiIndices(dtiobj.smooth)
R> tracks <- tracking(dtiobj, minfa = 0.2)
R> tracks <- reduceFibers(tracks, maxdist = 0.5)
R> tracks.smooth <- reduceFibers(tracking(dtiobj.smooth, minfa = 0.2),
+    maxdist = 0.5)
R> source(system.file("rcode/mousecallbacks.r", package = "dti"))
R> sx <- 400
R> sy <- 450
R> w1 <- show3d(dtiind, FOV = 1, windowRect = c(1, 1, sx, sy))
R> w2 <- show3d(dtiind.smooth, FOV = 1,
+    windowRect = c(sx + 11, 1, 2 * sx + 10, sy))
R> w3 <- show3d(tracks, FOV = 1,
+    windowRect = c(2 * sx + 21, 1, 3 * sx + 20, sy))
R> w4 <- show3d(tracks.smooth, FOV = 1,
+    windowRect = c(3 * sx + 31, 1, 4 * sx + 30, sy))
```

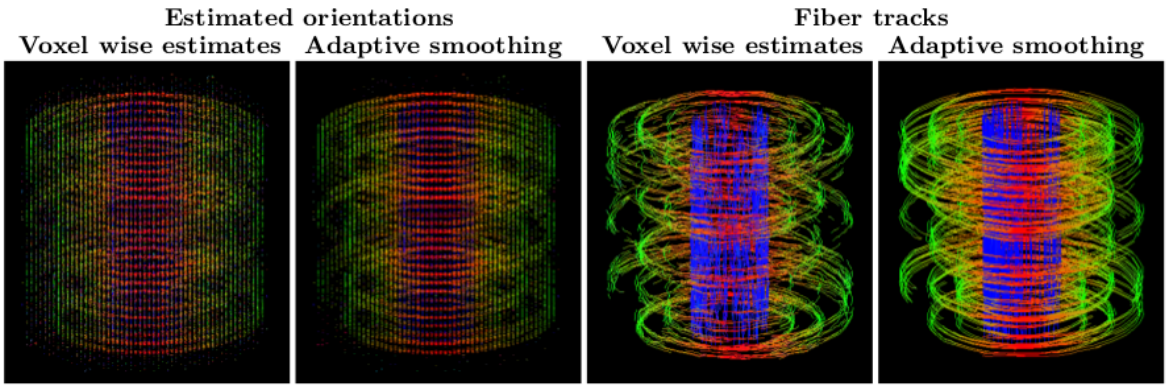

Figure 5: Example 4.1 (artificial data). 3D visualization of main tensor orientations without and with use of structural adaptive smoothing and corresponding fiber tracking results (from left to right). Results are shown for voxel with estimated FA > 0.3 and fiber tracks starting from such voxel. Color codes estimated directions as for FA maps.

```
R> mouseTrackball(dev = c(w1, w2, w3, w4))
R> mouseZoom(2, dev = c(w1, w2, w3, w4))
R> mouseFOV(3, dev = c(w1, w2, w3, w4))
R> cat("w1 - Fiber orientations from tensor estimates\n
+  w2 - Fiber orientations from smoothed tensor estimates\n
+  w3 - Tracking results from tensor estimates\n
+  w4 - Tracking results from smoothed tensor estimates\n
+  - Color codes orientation: red - along x; green - along y; blue - along z")
R> rgl.set(w1)
R> rgl.snapshot("ex1tens.png")
R> rgl.set(w2)
R> rgl.snapshot("ex1smtens.png")
R> rgl.set(w3)
R> rgl.snapshot("ex1tracks.png")
R> rgl.set(w4)
R> rgl.snapshot("ex1smtracks.png")
```

Figure 5 provides a 3D visualization of tensor characteristics and fiber tracking results. Orientations are color coded using Equation 3. Note the improvement of results due to adaptive smoothing.

4.2. Example: The effect of regularization in Q-ball imaging

The next example illustrates the effect of regularization in ODF reconstruction with spherical harmonics using the experimental data set 1. The data are modeled using a tensor mixture model of maximum order 4 and the ODF-estimate (5, 6) applying the regularization proposed in Aganj *et al.* (2010) when estimating the coefficients in (5). The regularization parameter is chosen as $\lambda_{reg} = \{2.5 \cdot 10^{-3}, 1 \cdot 10^{-2}, 4 \cdot 10^{-2}\}$, respectively.

```
R> gradients <- read.table("b-directions.txt")
R> dwiobj <- readDWIdata(gradients, "data1", "NIFTI")
```

```
R> dwiobj <- sdpar(dwiobj, 500, interactive = FALSE)
R> mtensobj <- dwiMixtensor(dwiobj, maxcomp = 4, pen = 1)
R> dwiqball8.25m3 <- dwiQball(dwiobj, order = 8, lambda = 2.5e-3)
R> dwiqball8.1m2 <- dwiQball(dwiobj, order = 8, lambda = 1e-2)
R> dwiqball8.4m2 <- dwiQball(dwiobj, order = 8, lambda = 4e-2)
```

Coordinates of two voxel with structure have been determined interactively using

```
R> coord <- plot(mtensobj, slice = 3, what = "eorder", view = "axial",
+    identify = TRUE)
```

Get coordinates of two interesting voxel; here: `c(23, 23, 3)` (inside a large region of estimated order 2 voxel) and `c(10, 16, 3)` (an estimated order 3 voxel). These voxels have been used in the two rows of Figure 6.

```
R> source(system.file("rcode/mousecallbacks.r", package = "dti"))
R> sx <- 400
R> sy <- 400
R> w1 <- show3d(mtensobj[23, 23, 3], windowRect = c(1, 1, sx, sy))
R> w2 <- show3d(dwiqball8.25m3[23, 23, 3],
+    windowRect = c(sx + 11, 1, 2 * sx + 10, sy))
R> w3 <- show3d(dwiqball8.1m2[23, 23, 3],
+    windowRect = c(2 * sx + 21, 1, 3 * sx + 20, sy))
R> w4 <- show3d(dwiqball8.4m2[23,23,3],
+    windowRect = c(3 * sx + 31, 1, 4 * sx + 30, sy))
R> mouseTrackball(dev = c(w1, w2, w3, w4))
R> mouseZoom(2,dev = c(w1, w2, w3, w4))
R> mouseFOV(3,dev = c(w1, w2, w3, w4))
R> rgl.set(w1)
R> rgl.snapshot("ex2mix2.png")
R> rgl.set(w2)
R> rgl.snapshot("ex2qball2a.png")
R> rgl.set(w3)
R> rgl.snapshot("ex2qball2b.png")
R> rgl.set(w4)
R> rgl.snapshot("ex2qball2c.png")
R> w5 <- show3d(mtensobj[10, 16, 3],
+    windowRect = c(1, sy + 11, sx, 2 * sy + 10))
R> w6 <- show3d(dwiqball8.25m3[10, 16, 3],
+    windowRect = c(sx + 11, sy + 11, 2 * sx + 10, 2 * sy + 10))
R> w7 <- show3d(dwiqball8.1m2[10, 16, 3],
+    windowRect = c(2 * sx + 21, sy + 11, 3 * sx + 20, 2 * sy + 10))
R> w8 <- show3d(dwiqball8.4m2[10, 16, 3],
+    windowRect = c(3 * sx + 31, sy + 11, 4 * sx + 30, 2 * sy + 10))
R> mouseTrackball(dev = c(w5, w6, w7, w8))
R> mouseZoom(2, dev = c(w5, w6, w7, w8))
R> mouseFOV(3, dev = c(w5, w6, w7, w8))
R> rgl.set(w5)
```

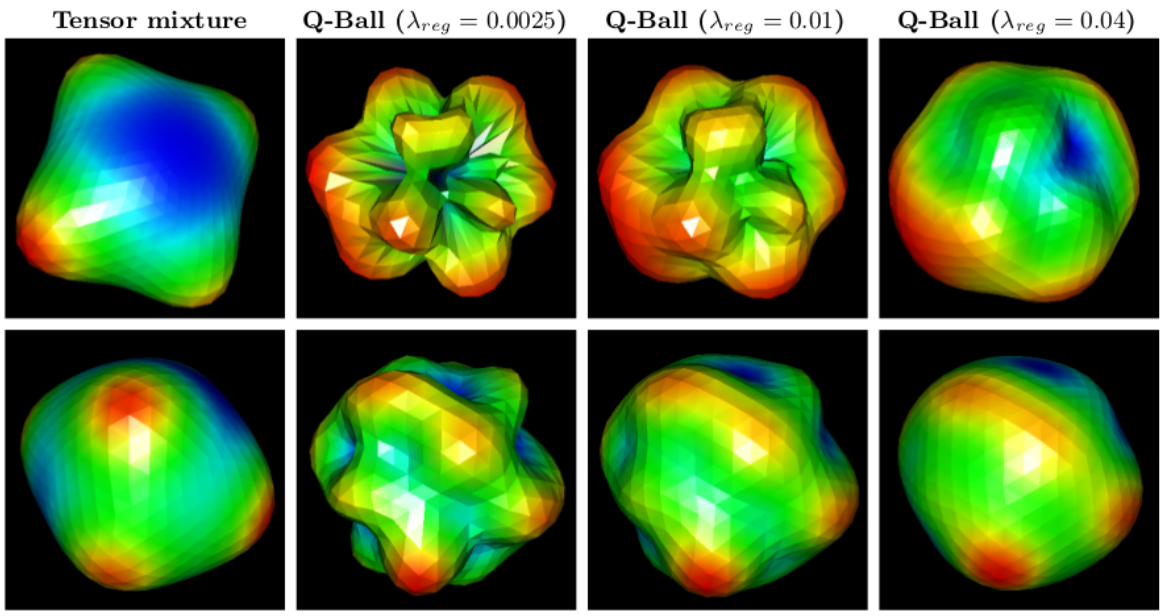

Figure 6: ODF estimated using tensor mixture models (left) and using ODF reconstruction with spherical harmonics of order 8 and regularization parameter $\lambda_{reg} = 2.5 \cdot 10^{-3}, 1 \cdot 10^{-2}, 4 \cdot 10^{-2}$ (from left to right) for two interactively selected voxel. Values of the estimated ODF are color coded. In contrast to color coded FA maps red and blue represent large and small values of the estimated ODF, respectively. Yellow and green correspond to intermediate values.

```
R> rgl.snapshot("ex2mix3.png")
R> rgl.set(w6)
R> rgl.snapshot("ex2qball3a.png")
R> rgl.set(w7)
R> rgl.snapshot("ex2qball3b.png")
R> rgl.set(w8)
R> rgl.snapshot("ex2qball3c.png")
```

Figure 6 illustrates results using a tensor mixture model and ODF reconstruction with spherical harmonics of order 8. Stronger regularization, for larger values of λ_{reg}, reduces the variability of the estimated ODF, at the cost of a possible bias.

ODF reconstruction using spherical harmonics is, as a solution of a linear problem, an appealing method. This comes at the cost of a biased estimate due a violation of its mono-exponential decay assumption. Adequate modeling may be achieved using multi-shell acquisition schemes that lead to a multi-exponential decay assumption (Descoteaux *et al.* 2010; Aganj *et al.* 2010). The method requires one to choose appropriate parameters l and λ_{reg}.

4.3. Example: Tensor mixture models

Here, we illustrate capabilities of the tensor mixture model in comparison to the single tensor model. We first analyze the experimental data set 2 with both models.

```
R> gradients <- read.table("b-directions.txt")
```

```
R> dwiobj <- readDWIdata(gradients, "data2", "NIFTI")
R> dwiobj <- sdpar(dwiobj, 500, interactive = FALSE)
R> tensobj <- dtiTensor(dwiobj)
R> summary(tensobj)
R> indobj <- dtiIndices(tensobj)
R> summary(indobj)
R> mtobj1 <- dwiMixtensor(dwiobj, maxcomp = 1)
R> mtobj2 <- dwiMixtensor(dwiobj, maxcomp = 2)
R> mtobj2imp <- dwiMtImprove(mtobj2, dwiobj, maxcomp = 2)
R> mtobj2comb <- dwiMtCombine(mtobj2imp, mtobj1)
R> mtobj3 <- dwiMixtensor(dwiobj, maxcomp = 3)
R> mtobj3imp <- dwiMtImprove(mtobj3,dwiobj, maxcomp = 3)
R> mtobj3comb <- dwiMtCombine(mtobj3imp, mtobj2comb)
R> mtobj4 <- dwiMixtensor(dwiobj, maxcomp = 4)
R> mtobj4imp <- dwiMtImprove(mtobj4,dwiobj, maxcomp = 4)
R> mtobj4comb <- dwiMtCombine(mtobj4imp, mtobj3comb)
R> summary(mtobj4comb)
```

Parameter estimation in the tensor mixture model 8 requires one to solve a non-convex optimization problem. In such problems results depend on the appropriate choice of initial values for the parameters. The method `dwiMtImprove` allows for possible improvements using results from neighboring voxel for improved initial estimates. The method `dwiMtCombine` is used for a voxel-wise comparison of results from two `dwiMixtensor`-objects selecting the best reconstruction with respect to the specified model selection criterion (default: `"BIC"`). In the example these methods are effectively used to select, in each voxel, a best estimate using different initial parameters.

The method `extract` is now used to access components from the objects containing the tensor and tensor mixture estimates.

```
R> tensorfa <- extract(indobj, what = "fa")$fa
R> mtobjind <- extract(mtobj4comb,
+    what = c("fa", "order", "eorder", "ev", "mix"))
R> signif(quantile(tensorfa), 3)

    0%    25%    50%    75%   100%
0.0123 0.1120 0.3360 0.5120 0.8030

R> signif(quantile(mtobjind$fa), 3)

     0%     25%     50%     75%    100%
0.00997 0.10400 0.50900 0.78500 0.95700

R> table(mtobjind$order)

  1   2   3
457 448  85
```

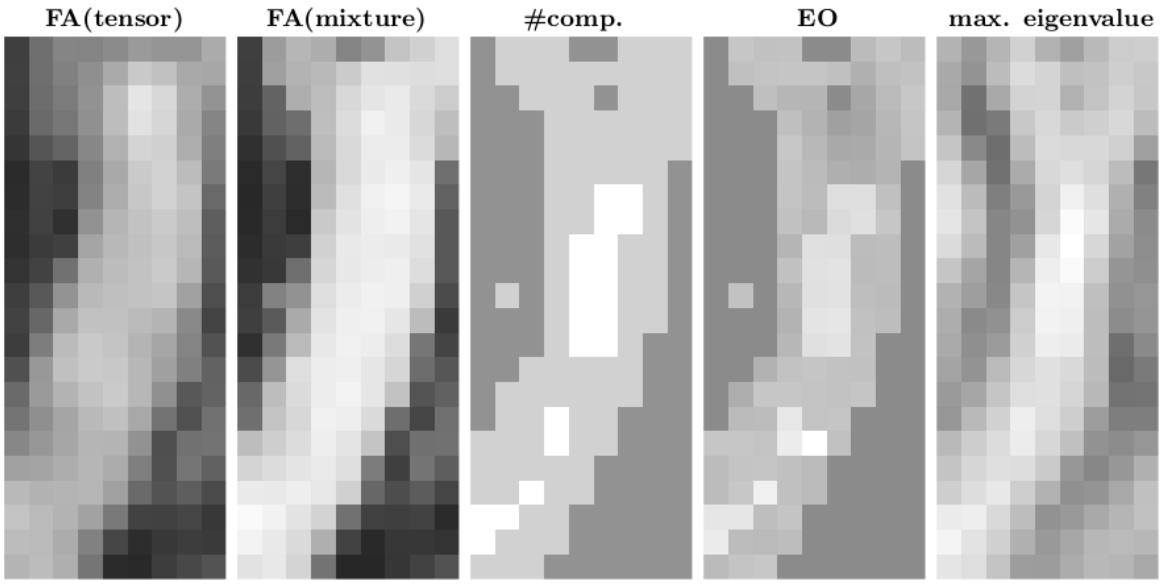

Figure 7: Visualization of results for the experimental data set 2, axial slice 2: FA (tensor model)(range $(0, 1)$), FA (tensor mixture model)(range $(0, 1)$), estimated number of mixture components (range $(0, 3)$), effective order (range $(0, 2.8)$) and maximal eigenvalue (range $(0, 2.27)$) for mixture model with maximum model order 4 (from left to right). FA values correspond to image intensity in both FA plots.

```
R> signif(quantile(mtobjind$eorder), 3)

  0%  25%  50%  75% 100%
1.00 1.00 1.57 1.87 2.91
```

The functions `plot`, `show.image` and `write.image` use capabilities of package **adimpro** (Polzehl and Tabelow 2007). Figure 7 is created by

```
R> tensorfa[tensorfa < 0.3] <- 0
R> img0 <- make.image(65535 * tensorfa[, , 2])
R> img1 <- plot(mtobj4comb, slice = 2, what = "fa", view = "axial")
R> img2 <- plot(mtobj4comb, slice = 2, what = "order", view = "axial")
R> img3 <- plot(mtobj4comb, slice = 2, what = "eorder", view = "axial")
R> img4 <- plot(mtobj4comb, slice = 2, what = "ev", view = "axial")
R> X11(width = 12, height = 6)
R> par(mfrow = c(1, 5), mar = c(1, 1, 3, 0.2), mgp = c(2, 1, 0))
R> show.image(img0, main = "Tensor FA")
R> show.image(img1, main = "Mixture FA")
R> show.image(img2, main = "Mixture order")
R> show.image(img3, main = "Effective order")
R> show.image(img4, main = "Maximum Eigenvalue")
R> write.image(img0, file = "ex3tensfa.png")
R> write.image(img1, file = "ex3mixfa.png")
R> write.image(img2, file = "ex3mixord.png")
```

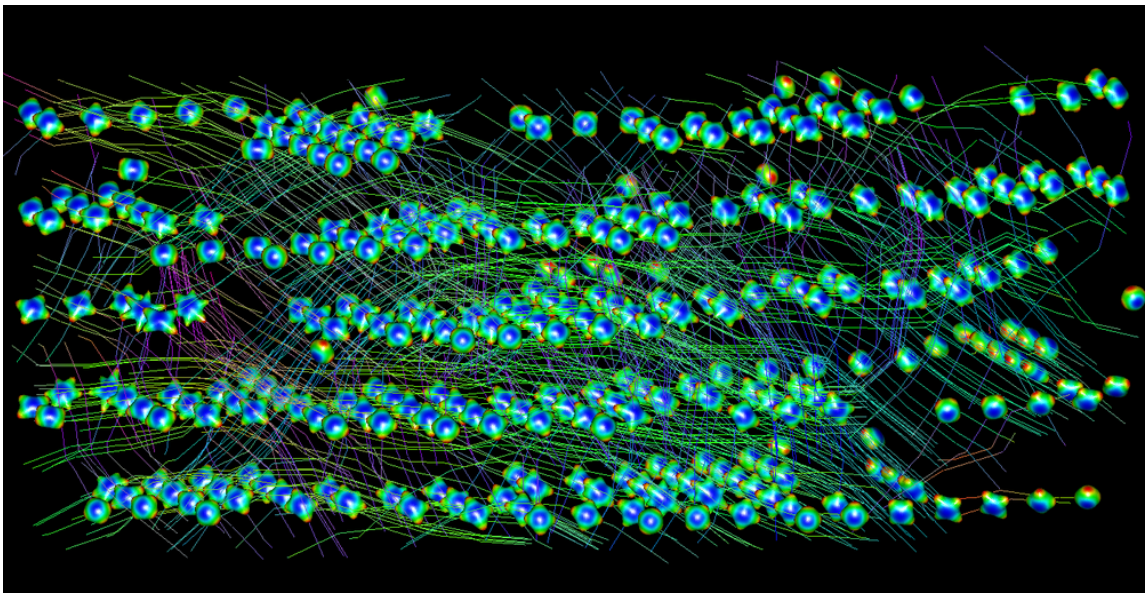

Figure 8: 3D visualization of results for the experimental data set 2: Voxel with estimated effective order larger than 1.8 and fiber tracks starting within these voxels. Figure 3 (right) illustrates the location of this region within the brain.

```
R> write.image(img3, file = "ex3mixeo.png")
R> write.image(img4, file = "ex3mixev.png")
```

provides characteristics of results obtained in the analysis. The left image shows the FA for the second axial slice obtained using the tensor model. The other four images provide FA, estimated number of mixture components, effective order and maximal eigenvalues (from left to right) for the same slice obtained employing a tensor mixture model with specified maximal number of compartments of 4 (see Tabelow *et al.* 2011b, for definitions and details). We observe an increase of FA in comparison with the tensor model, especially in regions adjacent to tissue borders. Note the spatial homogeneity observed in all characteristics for the tensor mixture model.

```
R> w1 <- show3d(mtobj4comb, maxangle = 45, fibers = TRUE, mineo = 1.8,
+    maxobjects = 990, FOV = 1, windowRect = c(1, 1, 1400, 720), lwd = 3)
R> rgl.snapshot("eo1.8regionmix5.png")
```

Figure 8 illustrated some capabilities in 3D visualization. The image shows estimated ODF's for all voxel with effective order larger or equal than 1.8 together with fiber tracks starting from these voxel. The data are rotated to show the five slices as individual layers. Color codes values for the estimated ODF and direction for fiber tracks.

4.4. Example: Fiber tracking

The object `tracks3.100` provided in file `tracks3_100.rsc` has been obtained analyzing high resolution DWI data recorded by H.-U. Voss at Weill Medical College, Cornell University NY. 140 gradient directions were used and images of $256 \times 256 \times 66$ voxel with spatial resolution

of approximately 0.9 mm ×0.9 mm ×1.8 mm where recorded. Fiber tracking is performed by the method `tracking`. The R code

```
R> load("tracks3_100.rsc")
R> summary(tracks3.100)
```

provides a complete history of the object `tracks3.100` including the applied functions and methods for the tracking and the basic characteristics of the object:

```
  Object of class dwiFiber
  Generated by calls    :
[[1]]
readDWIdata(gradient, "s0004", "DICOM", 66, level = 0.75)
...
[[8]]
selectFibers(nymix3tracksred, minlength = 100)
  Source-Filename       : s0004
  Dimension             : 186x243x66
  Number of Gradients   : 150
  Voxel extensions      : 0.8984x0.8984x1.8
  Minimum FA  : 0.266
  Maximum angle : 45
  Number of fibers : 8278
  Quantiles of fiber lengths:
  0%  25%  50%  75% 100%
 100  111  126  149  311
  Total number of line segments : 1104254
```

Figure 9 is generated by

```
R> w1 <- show3d(tracks3.100, windowRect = c(1, 1, 900, 800), bg = "white")
R> w2 <- show3d(tracks3.100, windowRect = c(901, 1, 1900, 800), bg = "white")
R> rgl.set(w1)
R> rgl.snapshot("tracks100a.png")
R> rgl.set(w2)
R> rgl.snapshot("tracks100b.png")
```

and provides an illustration of the main long fiber tracks revealed by the analysis. Images have been rotated into the correct position before `rgl.snapshot` was used. Annotations where then made using **GIMP** (The **GIMP** Team 2011).

5. Conclusions

With the package **dti** we provide a toolbox for the analysis of diffusion weighted MR data within the R language and environment for statistical computing (R Development Core Team 2011). The package includes functions for reading image data in DICOM and NIfTI format. The data can be analyzed using diffusion tensor models, tensor mixture models and ODF

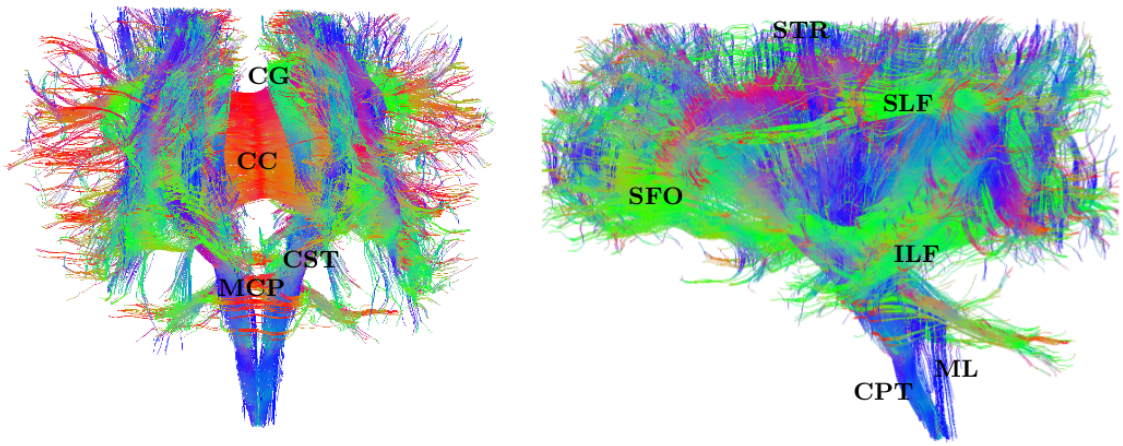

Figure 9: Visualization of fiber tracks with minimal length 100. Left image: view from posterior, right: sagittal view. Color codes the local direction of the fiber tracks using the same scheme as for the FA maps. We label some main tracks: corpus callosum (CC), cingulum (CG), superior fronto-occipital fasciculus (SFO), superior longitudinal fasciculus (SLF), superior thalamic radiation (STR), corticopontine tract (CPT), corticospinal tract (CST), medial cerebellar peduncle (MCP), medial lemniscus (ML), inferior longitudinal fasciculus (ILF). The upper slices of the brain were not scanned in favor of spinal cord slices.

models using spherical harmonics expansions. Fiber tracking may be performed using a deterministic streamline algorithm. The package has extensive 2D (based on the **adimpro** package, Polzehl and Tabelow 2007) and 3D (based on the **rgl** package, Adler and Murdoch 2010) visualization capabilities that can be used to produce publication ready illustrations. A special feature of the package are functions for model-based adaptive smoothing of DWI data. Further improvements will include a model free adaptive smoothing method and an OpenMP based parallel implementation. Alternatives for reading and writing image data are provided by **oro.dicom** (Whitcher 2011), **oro.nifti** (Whitcher *et al.* 2010, 2011), **tractor.base** (Clayden 2010; Clayden *et al.* 2011) and **Rniftilib** (Granert 2010). Interface functions to use capabilities of these packages are planned. We refer to Tabelow *et al.* (2011a) and the *Medical Imaging* task view (Whitcher 2010) for a comprehensive overview of related activities in R.

This paper discusses modeling for diffusion weighted MR experiments, describes the package structure and provides guidance for a typical analysis using several instructive examples. We encourage the reader to use the example R scripts and data provided as an electronic appendix to follow the analysis and to get an impression of the 3D visualization capabilities. The R scripts may also serve as a template for analyzing your own data.

Appendices

The electronic appendix contains the data sets used in directories `data1`, `data2`, `data3`, `data4a` and `data4b` as well as scripts containing the R code used to produce the figures ant to perform the analysis in the examples.

Acknowledgments

This work is supported by the DFG Research Center MATHEON. We thank H.U. Voss for agreeing to make the experimental data used in this paper publicly available under GPL ≥ 2. We thank two anonymous reviewers and the associate editor for their very constructive and helpful comments.

References

Adler D, Murdoch D (2010). ***rgl**: 3D Visualization Device System (OpenGL)*. R package version 0.92.794, URL http://CRAN.R-project.org/package=rgl.

Aganj I, Lenglet C, Jahanshad N, Yacoub E, Harel N, Thompson P, Sapiro G (2011). "A Hough Transform Global Probabilistic Approach to Multiple-Subject Diffusion MRI Tractography." *Medical Image Analysis*, **15**(4), 414–425.

Aganj I, Lenglet C, Sapiro G, Yacoub E, Ugurbil K, Harel N (2010). "Reconstruction of the Orientation Distribution Function in Single- and Multiple-Shell Q-Ball Imaging Within Constant Solid Angle." *Magnetic Resonance in Medicine*, **64**(2), 554–556.

Alexander DC (2005). "Multiple-Fiber Reconstruction Algorithms for Diffusion MRI." *The Annals of the New York Acadamy of Sciences*, **1064**, 113–133.

Alexander DC (2006). "An Introduction to Computational Diffusion MRI: The Diffusion Tensor and Beyond." In J Weickert, H Hagen (eds.), *Visualization and Image Processing of Tensor Fields*. Springer-Verlag.

Anderson A (2005). "Measurements of Fiber Orientation Distributions Using High Angular Resolution Diffusion Imaging." *Magnetic Resonance in Medicine*, **54**(5), 1194–1206.

Barnett A (2009). "Theory of Q-Ball Imaging Redux: Implications for Fibre Tracking." *Magnetic Resonance in Medicine*, **62**(4), 910–923.

Basser PJ, Jones DK (2002). "Diffusion-Tensor MRI: Theory, Experimental Design and Data Analysis – A Technical Review." *NMR in Biomedicine*, **15**, 456–467.

Basser PJ, Mattiello J, Le Bihan D (1994a). "Estimation of the Effective Self-Diffusion Tensor from the NMR Spin Echo." *Journal of Magnetic Resonance B*, **103**(3), 247–254.

Basser PJ, Mattiello J, Le Bihan D (1994b). "MR Diffusion Tensor Spectroscopy and Imaging." *Biophysical Journal*, **66**(1), 259–267.

Behrens TEJ, Johansen-Berg H, Jbabdi S, Rushworth MFS, Woolrich MW (2007). "Probabilistic Diffusion Tractography with Multiple Fibre Orientations: What Can We Gain?" *NeuroImage*, **34**(1), 144–155.

Callaghan PT (1991). *Principles of Nuclear Magnetic Resonance Microscopy*. Oxford Science Publications.

Chambers JM (2008). *Software for Data Analysis: Programming with R*. Statistics and Computing. Springer-Verlag.

Clark CA, Barker GJ, Tofts PS (1999). "Magnetic Resonance Diffusion Imaging of the Human Cervical Spinal Cord in Vivo." *Magnetic Resonance in Medicine*, **41**(6), 1269–1273.

Clayden J (2010). ***tractor.base**: A Package for Reading, Manipulating and Visualising Magnetic Resonance Images*. R package version 1.6-0, URL http://CRAN.R-project.org/package=tractor.base.

Clayden JD, Muñoz Maniega S, Storkey AJ, King MD, Bastin ME, Clark CA (2011). "**TractoR**: Magnetic Resonance Imaging and Tractography with R." *Journal of Statistical Software*, **44**(8), 1–18. URL http://www.jstatsoft.org/v44/i08/.

Deppe M, Kellinghaus C, Duning T, Moddel G, Mohammadi S, Deppe K, Schiffbauer H, Kugel H, Keller SS, Ringelstein EB, Knecht S (2008). "Nerve Fiber Impairment of Anterior Thalamocortical Circuitry in Juvenile Myoclonic Epilepsy." *Neurology*, **71**(24), 1981–1985.

Descoteaux M, Angelino E, Fitzgibbons S, Deriche R (2007). "Regularized, Fast and Robust Analytical Q-Ball Imaging." *Magnetic Resonance in Medicine*, **58**(3), 497–510.

Descoteaux M, Deriche R, Knösche TR, Anwander A (2009). "Deterministic and Probabilistic Tractography Based on Complex Fiber Orientation Distributions." *IEEE Transactions on Medical Imaging*, **28**(2), 269–286.

Descoteaux M, Deriche R, Le Bihan D, Mangin JF, Poupon C (2010). "Multiple q-Shell Diffusion Propagator Imaging." *Medical Image Analysis*, **15**(4), 603–621.

Duning T, Kellinghaus C, Mohammadi S, Schiffbauer H, Keller SS, Ringelstein EB, S K, Deppe M (2010). "Individual White Matter Fractional Anisotropy Analysis on Patients with MRI-Negative Partial Epilepsy." *Journal of Neurology, Neurosurgery & Psychiatry with Practical Neurology*, **81**(2), 136–139.

Granert O (2010). ***Rniftilib**: R Interface to **NIFTICLIB***. R package version 1.1-0, URL http://CRAN.R-project.org/package=Rniftilib.

Hankin RKS (2006). "Special Functions in R: Introducing the **gsl** Package." *R News*, **6**(4), 24–26. URL http://CRAN.R-project.org/doc/Rnews/.

Hess C, Mukherjee P, Han E, Xu D, Vigneron D (2006). "Q-Ball Reconstruction of Multimodal Fiber Orientations Using the Spherical Harmonic Basis." *Magnetic Resonance in Medicine*, **56**(1), 104–117.

Johansen-Berg H, Behrens TEJ (2009). *Diffusion MRI: From Quantitative Measurement to In-Vivo Neuroanatomy*. Academic Press.

Kellinghaus C, Deppe M, Duning T, Kugel H, Mohammadi S, Knecht S (2006). "Diffusion Tensor Imaging in Patients with Juvenile Myoclonic Epilepsy." *Epilepsia*, **47**(S4), 71.

Kleffner I, Deppe M, Mohammadi S, Schiffbauer H, Stupp N, Lohmann H, Young P, Ringelstein EB (2008). "Diffusion Tensor Imaging Demonstrates Fiber Impairment in Susac Syndrome." *Neurology*, **70**(19 Pt 2), 1867–1869.

Le Bihan D, Breton E (1985). "Imagerie de Diffusion in Vivo par Résonance Magnétique Nucléaire (In Vivo Magnetic Resonance Imaging of Diffusion)." *Comptes rendus de l'Académie des Sciences. La vie des sciences*, **301**, 1109–1112.

Le Bihan D, Mangin JF, Poupon C, Clark CA, Pappata S, Molko N, Chabriat H (2001). "Diffusion Tensor Imaging: Concepts and Applications." *Journal of Magnetic Resonance*, **13**(4), 534–546.

Leow A, Zhu S, McMahon K, de Zubicaray G, Meredith M, Wright M, Thompson P (2009). "The Tensor Distribution Function." *Magnetic Resonance in Medicine*, **61**(1), 205–214.

Mardia KV, Jupp PE (2000). *Directional Statistics*. John Wiley & Sons.

Merboldt KD, Hanicke W, Frahm J (1985). "Self-Diffusion NMR Imaging Using Stimulated Echoes." *Journal of Magnetic Resonance*, **64**(3), 479–486.

Mori S, Crain BJ, Chacko VP, van Zijl PCM (1999). "Three Dimensional Tracking of Axonal Projections in the Brain by Magnetic Resonance Imaging." *The Annals of Neurology*, **45**(2), 265–269.

Mori S, van Zijl PCM (2002). "Fibre Tracking: Principles and Strategies – A Technical Review." *NMR in Biomedicine*, **15**(7-8), 468–480.

Özarslan E, Shepherd TM, Vemuri BC, Blackband SJ, Mareci TH (2006). "Resolution of Complex Tissue Microarchitecture Using the Diffusion Orientation Transform (DOT)." *NeuroImage*, **31**, 1086–1103.

Polzehl J, Tabelow K (2007). "Adaptive Smoothing of Digital Images: The R Package **adimpro**." *Journal of Statistical Software*, **19**(1), 1–17. URL http://www.jstatsoft.org/v19/i01/.

Polzehl J, Tabelow K (2009). "Structural Adaptive Smoothing in Diffusion Tensor Imaging: The R Package **dti**." *Journal of Statistical Software*, **31**(9), 1–23. URL http://www.jstatsoft.org/v31/i09/.

R Development Core Team (2011). *R: A Language and Environment for Statistical Computing*. R Foundation for Statistical Computing, Vienna, Austria. ISBN 3-900051-07-0, URL http://www.R-project.org/.

Reisert M, Mader I, Anastasopoulos C, Weigel M, Schnell S, Kiselev V (2011). "Global Fiber Reconstruction Becomes Practical." *NeuroImage*, **54**(2), 955–962.

Schwarz G (1978). "Estimating the Dimension of a Model." *The Annals of Statistics*, **6**(2), 461–464.

Sinha S, Sinha U, Edgerton VR (2006). "In Vivo Diffusion Tensor Imaging of the Human Calf Muscle." *Journal of Magnetic Resonance Imaging*, **24**(1), 182–190.

Smith SM, Johansen-Berg H, Jenkinson M, Rueckert D, Nichols TE, Miller KL, Robson MD, Jones DK, Klein JC, Bartsch AJ, Behrens TEJ (2007). "Acquisition and Voxelwise Analysis of Multi-Subject Diffusion Data with Tract-Based Spatial Statistics." *Nature Protocols*, **2**, 499–503.

Stejskal EO, Tanner JE (1965). "Spin Diffusion Measurements: Spin Echoes in the Presence of a Time-Dependent Field Gradient." *The Journal of Chemical Physics*, **42**(1), 288–292.

Tabelow K, Clayden JD, Lafaye de Micheaux P, Polzehl J, Schmid VJ, Whitcher B (2011a). "Image Analysis and Statistical Inference in Neuroimaging with R." *NeuroImage*, **55**(4), 1686–1693.

Tabelow K, Polzehl J (2011). ***dti**: DTI/DWI Analysis*. R package version 0.9-6.3, URL http://CRAN.R-project.org/package=dti.

Tabelow K, Polzehl J, Spokoiny V, Voss HU (2008). "Diffusion Tensor Imaging: Structural Adaptive Smoothing." *NeuroImage*, **39**(4), 1763–1773.

Tabelow K, Voss HU, Polzehl J (2011b). "Modeling the Orientation Distribution Function by Mixtures of Angular Central Gaussian Distributions." *Journal of Neuroscience Methods*. doi:10.1016/j.jneumeth.2011.09.001.

Taylor DG, Bushell MC (1985). "The Spatial Mapping of Translational Diffusion Coefficients by the NMR Imaging Technique." *Physics in Medicine and Biology*, **30**(4), 345–349.

The **GIMP** Team (2011). "**GIMP** – The GNU Image Manipulation Program." Version 2.6, URL http://gimp.org/.

Tournier JD, Calamante F, Gadian DG, Connelly A (2004). "Direct Estimation of the Fiber Orientation Density Function from Diffusion-Weighted MRI Data Using Spherical Deconvolution." *NeuroImage*, **23**(3), 1176–1185.

Tuch DS (2002). *Diffusion MRI of Complex Tissue Structure*. Ph.D. thesis, Massachusetts Institute of Technology.

Tuch DS (2004). "Q-Ball Imaging." *Magnetic Resonance in Medicine*, **52**(6), 1358–1372.

Tuch DS, Reese TG, Wiegell MR, Makris N, Belliveau JW, Wedeen VJ (2002). "High Angular Resolution Diffusion Imaging Reveals Intravoxel White Matter Fiber Heterogeneity." *Magnetic Resonance in Medicine*, **48**(4), 577–582.

Wedeen VJ, Hagmann P, Tseng WY, Reese TG, Weisskopf RM (2005). "Mapping Complex Tissue Architecture with Diffusion Spectrum Imaging." *Magnetic Resonance in Medicine*, **54**(6), 1377–1386.

Whitcher B (2010). "CRAN Task View: Medical Image Analysis." Version 2010-11-30, URL http://CRAN.R-project.org/view=MedicalImaging.

Whitcher B (2011). ***oro.dicom**: Rigorous – DICOM Input / Output*. R package version 0.2.9, URL http://CRAN.R-project.org/package=oro.dicom.

Whitcher B, Schmid V, Thornton A (2010). ***oro.nifti**: Rigorous – NIfTI Input / Output*. R package version 0.2.6, URL http://CRAN.R-project.org/package=oro.nifti.

Whitcher B, Schmid VJ, Thornton A (2011). "Working with the DICOM and NIfTI Data Standards in R." *Journal of Statistical Software*, **44**(6), 1–28. URL http://www.jstatsoft.org/v44/i06/.

Wu X, Xu Q, Xu L, Zhou J, Anderson AW, Ding Z (2009). "Genetic White Matter Fiber Tractography with Global Optimization." *Journal of Neuroscience Methods*, **184**(2), 375–379.

Wu YC, Alexander AL (2007). "Hybrid Diffusion Imaging." *NeuroImage*, **36**(3), 617–629.

Xue R, van Zijl PCM, Crain BJ, Solaiyappan M, Mori S (1999). "In Vivo Three-Dimensional Reconstruction of Rat Brain Axonal Projections by Diffusion Tensor Imaging." *Magnetic Resonance in Medicine*, **42**(6), 1123–1127.

Zhang F, Hancock ER, Goodlett C, Gerig G (2009). "Probabilistic White Matter Fiber Tracking Using Particle Filtering and von Mises-Fisher Sampling." *Medical Image Analysis*, **13**(1), 5–18.

Affiliation:

Jörg Polzehl, Karsten Tabelow
Weierstrass Institute for Applied Analysis and Stochastics
Mohrenstr. 39
10117 Berlin, Germany
E-mail: joerg.polzehl@wias-berlin.de,
karsten.tabelow@wias-berlin.de
URL: http://www.wias-berlin.de/projects/matheon_a3/

Journal of Statistical Software http://www.jstatsoft.org/
published by the American Statistical Association http://www.amstat.org/
Volume 44, Issue 12 *Submitted:* 2010-11-10
October 2011 *Accepted:* 2011-06-15